AD-A124 127 CONTACT-STRESS ANALYSIS OF ELASTIC-VISCOELASTIC INTERFACE CONDITIONS(U) GARRETT TURBINE ENGINE CO PHOENIX AZ J R SMYTH ET AL. DEC 82 21-4140(1) 1/1

UNCLASSIFIED N00014-80-C-0870 F/G 11/2 NL

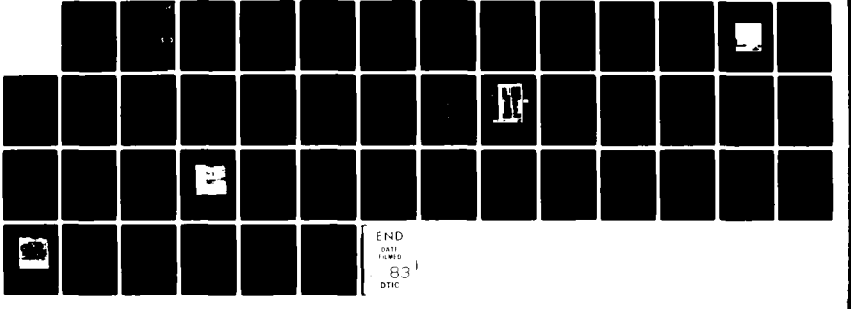

END

DATE FILMED

83

DTIC

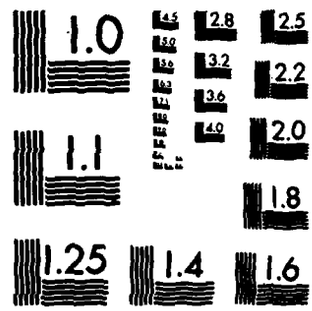

# CONTACT-STRESS ANALYSIS OF ELASTIC-VISCOELASTIC INTERFACE CONDITIONS

J.R. Smyth
D.W. Richerson

GARRETT TURBINE ENGINE COMPANY
A Division of the Garrett Corporation
111 South 34th Street, P.O. Box 5217
Phoenix, Arizona 85010

December 1982

Annual Technical Report
for the Period October 1981 to October 1982







Prepared for

OFFICE OF NAVAL RESEARCH
Department of the Navy
800 North Quincy Street
Arlington, Virginia 22217

SECURITY CLASSIFICATION OF THIS PAGE (When Data Entered)

## REPORT DOCUMENTATION PAGE

READ INSTRUCTIONS BEFORE COMPLETING FORM

| | |
|---|---|
| 1. REPORT NUMBER | 2. GOVT ACCESSION NO. AD-A124127 / 3. RECIPIENT'S CATALOG NUMBER |
| 4. TITLE (and Subtitle) CONTACT-STRESS ANALYSIS OF ELASTIC-VISCOELASTIC INTERFACE CONDITIONS | 5. TYPE OF REPORT & PERIOD COVERED Annual Report Oct 81 to Oct 82 |
| | 6. PERFORMING ORG. REPORT NUMBER 21-4140(1) |
| 7. AUTHOR(s) J.R. Smyth D.W. Richerson | 8. CONTRACT OR GRANT NUMBER(s) N00014-80-C-0870 |
| 9. PERFORMING ORGANIZATION NAME AND ADDRESS Garrett Turbine Engine Company 111 S. 34 St, P. O. Box 5217 Phoenix, AZ 85010 | 10. PROGRAM ELEMENT, PROJECT, TASK AREA & WORK UNIT NUMBERS |
| 11. CONTROLLING OFFICE NAME AND ADDRESS Office of Naval Research 800 N. Quincy St Arlington, VA 22217 | 12. REPORT DATE Dec 1982 |
| | 13. NUMBER OF PAGES 48 |
| 14. MONITORING AGENCY NAME & ADDRESS(if different from Controlling Office) | 15. SECURITY CLASS. (of this report) Unclassified |
| | 15a. DECLASSIFICATION/DOWNGRADING SCHEDULE |

16. DISTRIBUTION STATEMENT (of this Report)

Reproduction in whole or i[illegible] by the United States gover[illegible]

DISTRIBUTION STATEMENT A
Approved for public release;
Distribution Unlimited

[illegible] purpose

17. DISTRIBUTION STATEMENT (of the abstract entered in Block 20, if different from Report)

18. SUPPLEMENTARY NOTES

19. KEY WORDS (Continue on reverse side if necessary and identify by block number)

Contact Stress
Elastic-Viscoelastic Interface
High-Temperature Contact Testing

20. ABSTRACT (Continue on reverse side if necessary and identify by block number)

The sliding contact (frictional) behavior of Sintered Alpha Silicon Carbide (SASC) was studied over the range of room temperature to 1100°C. Both point- and line-contact configurations were evaluated under low normal forces. The results strongly indicate that a nonelastic mechanism is contributing to the contact behavior of SASC at elevated temperatures. The recovery force appears to be related to the magnitude of the

DD FORM 1 JAN 73 1473 EDITION OF 1 NOV 65 IS OBSOLETE

SECURITY CLASSIFICATION OF THIS PAGE (When Data Entered)

20. ABSTRACT (Continued)

nonelastic contribution. More experimental data is required to develop an analytical model to account for the nonelastic behavior at contact interfaces at elevated temperatures.

## PREFACE

This annual technical report was submitted by the Garrett Turbine Engine Company (GTEC), a Division of the Garrett Corporation, under Contract Number N00014-80-C-0870. The effort was sponsored by the Office of Naval Research, Arlington, Virginia, with Dr. R. Pohanka as Contract Monitor.

The following GTEC personnel contributed to the program:

| | |
|---|---|
| Program Managers | - J.M. Wimmer and P.M. Ardans, Propulsion Advanced Technology |
| Principal Investigators | - D.G. Finger, Mechanical Component Design, and D.W. Richerson, Advanced Materials |
| Technical Support | - J.R. Smyth, Advanced Materials |

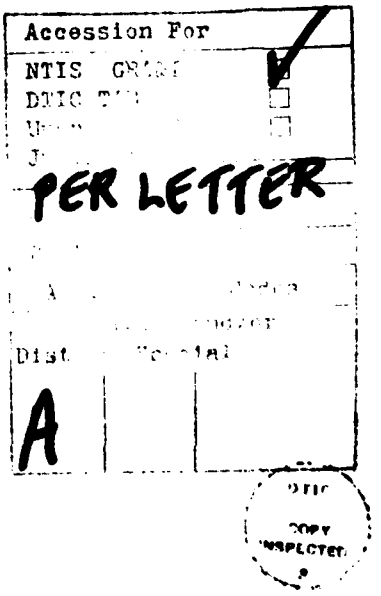

TABLE OF CONTENTS

# CONTACT-STRESS ANALYSIS OF ELASTIC-VISCOELASTIC INTERFACE CONDITIONS FINAL TECHNICAL REPORT

## 1.0 BACKGROUND

In the past, design methods and procedures for gas turbine engine components have been based on the use of ductile materials such as metals. However, in recent years numerous programs have focused on employing ceramics for high-temperature gas turbine engine components. Because of their brittle nature, ceramic components create unique design problems that require modified analytical techniques. Contact stress in ceramic-to-ceramic and ceramic-to-metal interfaces is one example of these problem areas. High, localized stresses do not redistribute in ceramics as they do in metal.

The Contact-Stress Analysis of Ceramic-to-Metal Interfaces Program was initiated under Office of Naval Research (ONR) funding in 1978 to systematically study contact interface phenomena. Since its inception, this program has involved an on-going study that blends analysis and specimen testing. All testing prior to 1982 was conducted at room temperature.

### 1.1 Room-Temperature Contact Testing and Analysis

The emphasis during the first year of this program centered on utilization of finite-element computer techniques, including zoom modeling, to effectively calculate the complex state of stress in the contact interface zone without compliant media. Frictional forces were identified as being the key to understanding contact behavior at ceramic interfaces.[1*]

*A list of references is presented in Section 6.

Work during the second year of the program focused on compliant media at the interface. The beneficial load-redistribution characteristics of compliant media were demonstrated through specimen testing and analysis using a finite-element approach. Specimen testing was also used to evaluate surface finish, machining direction, surface treatments, and compliant media durability. Over the load range examined in this program at room temperature, soft compliant layers such as platinum and fiber metals demonstrated more durability than materials with less compliance.[2]

The third year of the program focused on the effect of vibrational stresses on contact-surface failures. The stresses in this region are due to a complex interaction between contact and dynamic (vibrational) stresses. It was shown that as the contact loads increased, there was a corresponding decrease in the dynamic stresses at which failure occurred. It was concluded that the stresses due to contact forces combine with dynamic stresses to yield higher resultant stresses, causing the ceramic component to fail. The detrimental effect of contact loading decreases with decreasing contact force. It was also found that the use of compliant layers effectively decreases the detrimental effects of contact forces.[3]

Prior contact testing under the ONR program has been conducted at room temperature. As described in previous paragraphs, the ONR contact-stress program has achieved the development and verification of finite-element analysis for localized contact-stress distributions and has substantially increased our understanding of the effects of biaxial loading on fracture probability. However, parallel studies under the DARPA/NASC Ceramic Engine Demonstration Program[4,5] and the NASA/DOE Advanced Gas Turbine Program[6] have indicated that contact-stress mechanisms are different at elevated temperature for some ceramic materials, and that the finite-element analysis model developed under the

ONR program will require modification for these high-temperature conditions. Paragraph 1.2 describes the results of high-temperature tests under the DARPA/NASC and NASA/DOE Programs, the implications of these results on the current stress-analysis model, and additional studies that are required.

## 1.2 High-Temperature Contact Testing and Analysis

Tests were conducted on RBN104 Reaction-Bonded Silicon Nitride (RBSN)* and Sintered Alpha Silicon Carbide (SASC)* for both point contact and line contact at each of the following conditions: normal forces of 4.5, 11.4, and 26 kg; temperatures of 25°, 760°, 982°, and 1100°C. Figure 1 presents the curves for RBN104 and SASC at a normal force of 11.4 kg. At room temperature, the RBN104 RBSN has no clear delineation between the static and dynamic coefficients of friction. Optical and scanning electron microscopy (SEM) examinations of the contact surfaces show that surface cracking occurs, the surface finish of the moving specimen initially roughens, and a small mass of debris is pushed ahead of the contact. This results in the initial friction increase. However, some of this debris gets pulverized into a fine powder that apparently acts as a dry lubricant and begins to reduce the friction as the distance traversed increases. Roughening of the SASC also occurs at room temperature as a function of distance traversed, but the roughening occurs more slowly because SASC is harder and less porous than RBSN.

The nature of the friction curves is significantly different at elevated temperatures. At 982° and 1100°C, and to a slightly

*RBN104 Reaction-Bonded Silicon Nitride, AiResearch Casting Co., Torrance, CA. Sintered Alpha Silicon Carbide, Carborundum Co., Niagara Falls, NY.

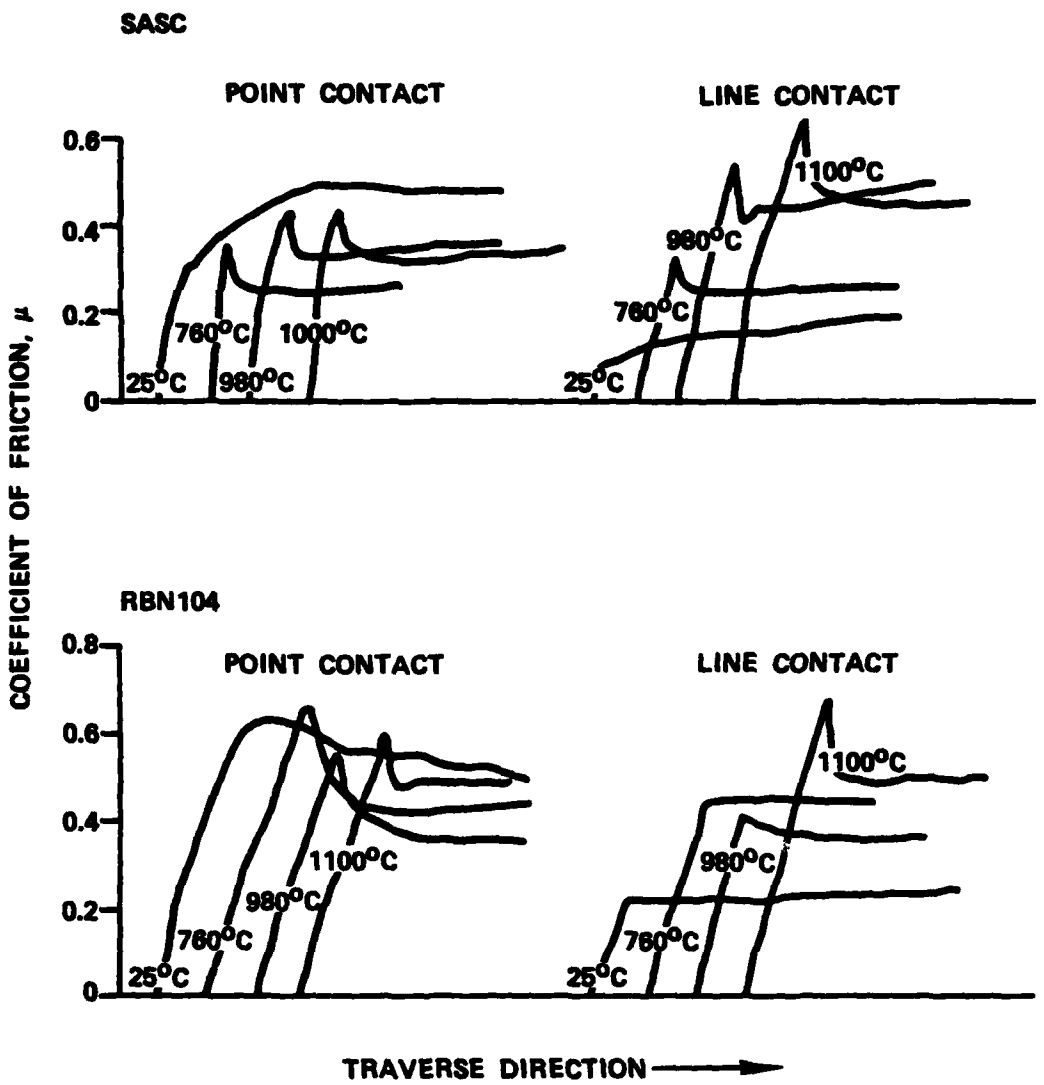


Figure 1. Force/Time Curves for 11.4-kg Normal Force Plotted in Terms of Coefficient of Friction Versus Distance Traversed. (Curves are superimposed to permit comparison.)

lesser extent at 760°C, both RBN104 and SASC have much higher static coefficients of friction than at 25°C; they also have a distinct breakaway. Optical and SEM examinations indicate that a glassy pool or layer, present at the contact surface, smeared during relative motion and accumulated along with some debr's ahead of the contact. This is shown in the scanning electron photomicrograph for SASC in Figure 2. Apparently, the glass forms due to surface oxidation (likely accelerated either by increased chemical activity due to the high local stress or by some other mechanism) and initially bonds the interface together. This explains the higher static coefficient of friction at high temperature and the distinct breakaway.

Figure 1 also compares the friction curves of RBN104 and SASC for line contact as a function of temperature. Under line contact, the two materials have similar friction characteristics, particularly at 1100°C. As with point contact, the effects of viscous glass at the contact surface appear to dominate behavior.

Friction data are useful but not as important as residual-strength data. The residual-strength measurement quantifies the amount of surface damage resulting from the contact conditions, and defines the subsequent tensile or flexural force range that a damaged component could withstand in service.

Table 1 summarizes the room-temperature, four-point bend strength of the stationary specimens from the contact tests of RBN104 and SASC described in Figure 1. It is evident that RBSN exhibits lower residual strength than SASC and that point contact results in lower strength than line contact. Specifically, the RBN104 exposed to point-contact biaxial loading has a residual strength of 121 MPa. Since the strength of this material prior to contact exposure typically ranges from 310 to 345 MPa, strength degradation for RBN104 is approximately 60 percent.

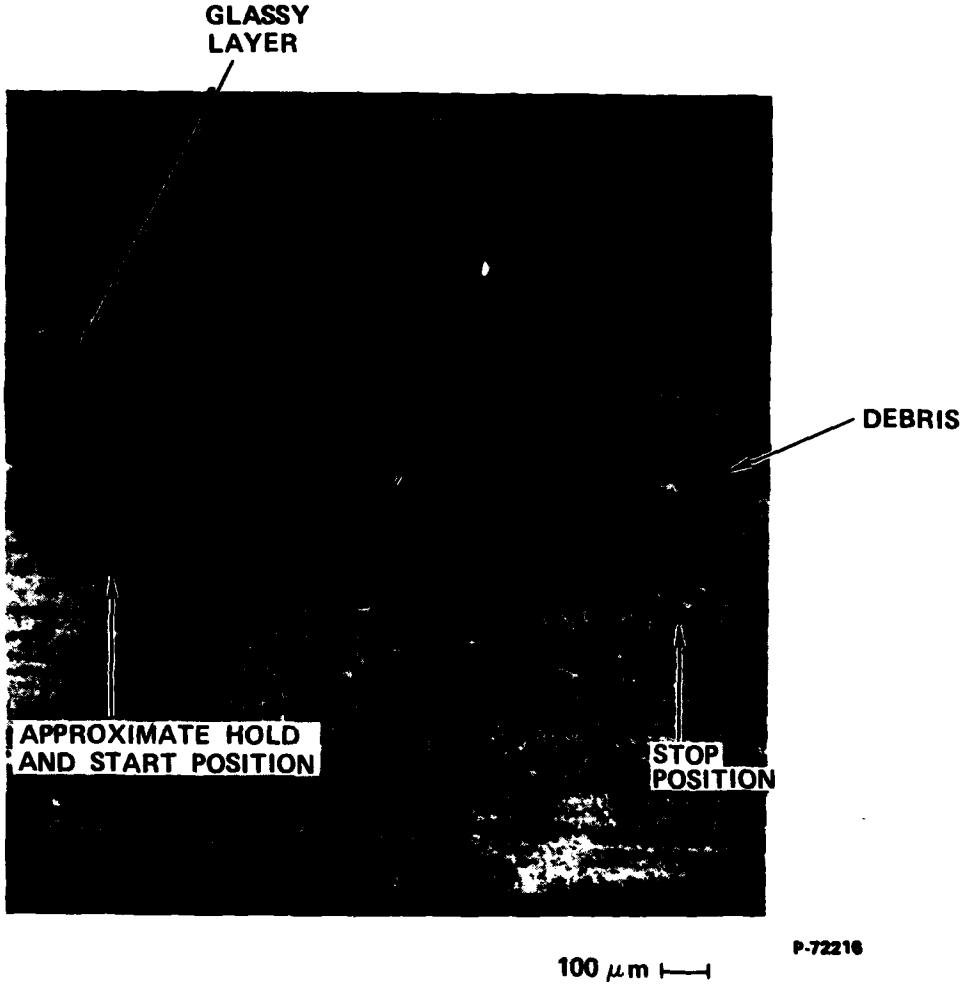


Figure 2. Scanning Electron Photomicrograph Showing Contact-Surface Features for SASC Tested at 1100°C, 11.4-kg Normal Force.

TABLE 1. ROOM-TEMPERATURE STRENGTHS AFTER LINE- AND POINT-CONTACT TESTS AT 26-KG NORMAL FORCE.

| Material | Contact | Contact Test Temperature (°C) | Average 4-Point Flexure Strength (MPa) |
|---|---|---|---|
| RBN104 | Point | 1100 | 121 |
| | Line | 1100 | 186 |
| SASC | Point | 1100 | 258 |
| | Line | 1100 | 433 |

Table 1 shows that SASC has higher residual strength than RBSN. Specifically, the average strength of SASC after point-contact biaxial loading is 258 MPa. Since the average strength prior to contact exposure is approximately 450 MPa strength degradation for SASC is approximately 43 percent for point contact and 4 percent for line contact.

To estimate the actual tensile stresses applied at the ceramic surfaces during biaxial contact loading, the contact test data for RBN104 and SASC were analyzed by the computer program developed in Reference 1. The results for room-temperature and 1100°C point- and line-contact conditions are summarized in Table 2. The 1100°C data are plotted in Figure 3 and compared with baseline four-point, flexure-strength data for the line-contact configuration.* In each case, the analysis predicts that the peak tensile stress for the sliding 26-kg normal force substantially exceeds the baseline material strength and, therefore, should result in considerable surface damage and strength reduction. Substantial strength reduction does occur for the point-contact condition with both materials and for the line-contact condition with RBSN, but it does not occur for the SASC line contact.

*Specimen oriented in the four-point test fixture with the flat surface in tension and the 0.63-cm radius surface in compression.

TABLE 2. PREDICTED CONTACT TENSILE STRESSES FOR POINT- AND LINE-CONTACT CONDITIONS.

| Material | Normal Load (kg) | Contact Test Temperature (°C) | Point Contact | | Line Contact | |
|---|---|---|---|---|---|---|
| | | | $\mu_s$* | $\sigma p$** (MPa) | $\mu_s$* | $\sigma p$** (MPa) |
| RNB104 RBSN | 4.5 | Room Temperature | 0.62 | 1020 | 0.18 | 71 |
| | 11.4 | Room Temperature | 0.62 | 1510 | 0.22 | 140 |
| | 26.0 | Room Temperature | 0.64 | 2020 | 0.22 | 213 |
| | 4.5 | 1100 | 0.64 | 1050 | 0.54 | 219 |
| | 11.4 | 1100 | 0.60 | 1460 | 0.68 | 440 |
| | 26.0 | 1100 | 0.52 | 1630 | 0.53 | 520 |
| SASC | 4.5 | Room Temperature | 0.25 | 460 | 0.25 | 137 |
| | 11.4 | Room Temperature | 0.19 | 530 | 0.09 | 74 |
| | 26.0 | Room Temperature | 0.26 | 1060 | 0.15 | 196 |
| | 4.5 | 1100 | 0.66 | 1170 | 0.62 | 32 |
| | 11.4 | 1100 | 0.51 | 1380 | 0.61 | 515 |
| | 26.0 | 1100 | 0.51 | 2000 | 0.70 | 900 |

*$\mu_s$ - static coefficient of friction

**$\sigma_p$ - calculated peak tensile stress

For SASC, the analysis predicts a peak tensile stress of 900 MPa, compared to a baseline material strength of 450 MPa and a retained strength of 433 MPa after biaxial contact exposure. This would suggest that, in the case of SASC at 1100°C, the actual contact stress is lower than the calculated stress. The current analysis and all prior reported analyses assume elastic conditions at the ceramic-to-ceramic interface. If a viscous layer is present at the interface, as the evidence indicates, a new analytical model must be prepared that includes both elastic and nonelastic terms.

Elastic stress distributions under static contact and sliding contact can be determined by either closed-form equations or finite-element analysis by utilizing existing or easily measured properties, i.e., the elastic modulus, Poisson's ratio and contact geometry of the two materials, the normal force, and in the latter case, the coefficient of friction or the tangential load.

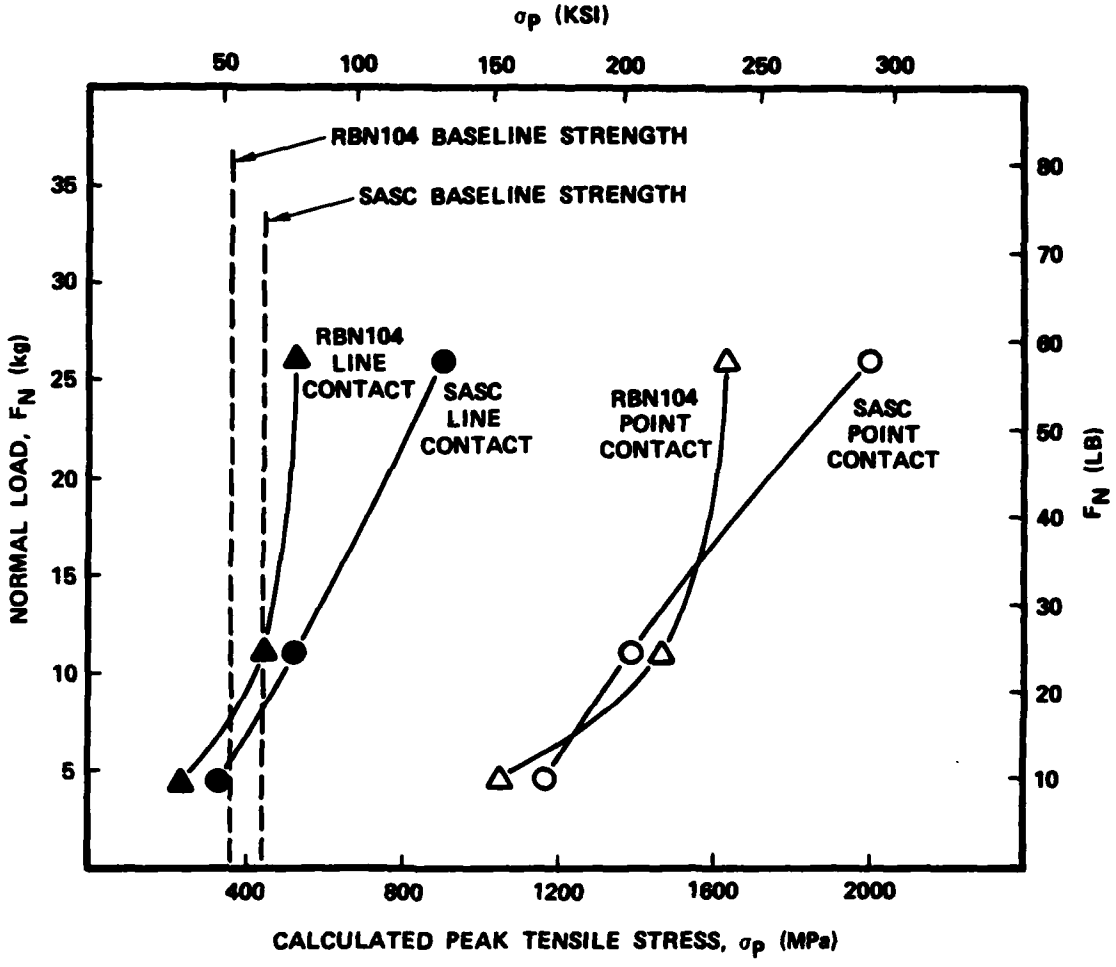


Figure 3. Calculated Peak Tensile Stresses for 1100°C Contact Tests.

The stress distribution will be more difficult to determine for the case of a viscous layer present at the contact interface. It is anticipated that the following conditions should be considered:

- o Viscosity of the interface material
- o Thickness and/or distribution of the viscous material
- o Temperature dependence of the viscosity
- o Load distribution in the viscous material (e.g., does the viscous material act like a compliant layer and spread the load over a larger area than the elastic contact region?)
- o Effect of area on shear load transfer and load distribution
- o Split between elastic and viscous effects on the measured coefficient of friction

It is apparent that the viscosity and distribution of the interface material and the relative split between elastic and viscous effects must be determined. This can be achieved by a combination of experimentation and analysis conducted in an iterative fashion to evolve an understanding of the elastic-nonelastic contact condition and to develop an analytical model.

A logical experimental approach to separate the elastic and viscous effects is to conduct elevated-temperature sliding tests at *decreasing* normal force and measure the tangential force required to initiate sliding. As the normal force decreases, the percent of elastic effect should decrease and the percent of viscous effect should correspondingly increase.

Some preliminary contact tests were conducted. SASC was tested at room temperature and 1100°C at normal forces of 2.0 and 1.4 kg. The data are plotted in Figure 4 along with data for normal forces of 11.4 and 4.5 kg. The tangential force increases dramatically relative to the normal force as the normal force decreases, resulting in very high apparent coefficient of friction. This strongly supports the hypothesis that a viscous interface material is present. The curve shapes in Figure 4 are estimated based upon the 11.4-kg data. Additional testing at intermediate temperatures is necessary to determine the actual friction-versus-temperature curves.

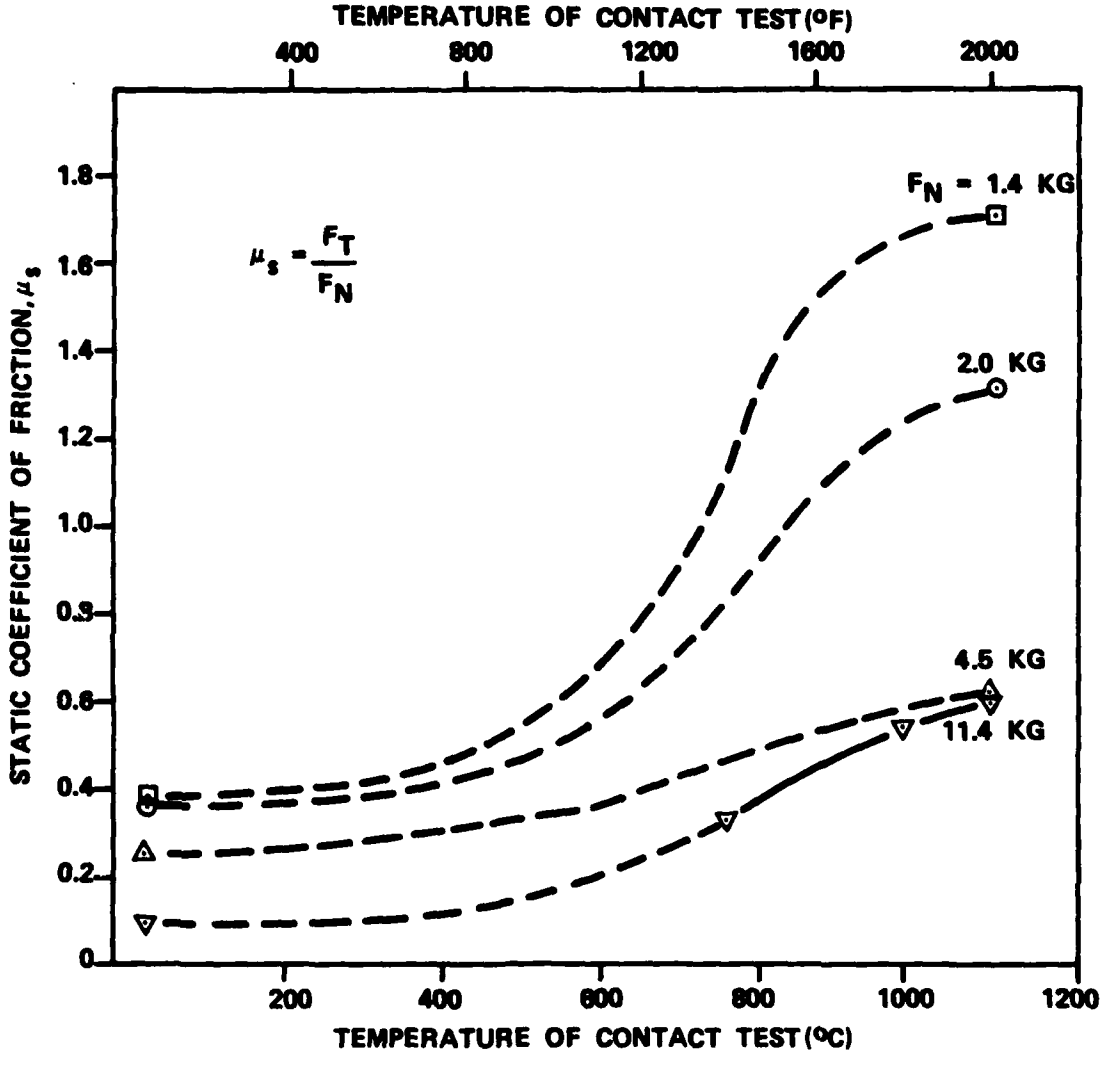


Figure 4. Static Coefficient of Friction for SASC as Function of Temperature and Normal Force.

## 2.0 EXPERIMENTAL PROGRAM CONDITIONS

The present experimental program was designed to study the contact behavior at elevated temperatures and attempt to separate the elastic and nonelastic effects. This study required testing at low contact loads and the ability to do many tests at elevated temperatures. To ensure reproducibility and allow for more rapid heating to high temperatures, the contact test rig and furnace were redesigned and constructed using company funds (refer to Section 3.0).

For this study, SASC test specimens were evaluated primarily in line contact over the temperature range of room temperature to 1100°C. The normal forces applied were 0.5, 1.4, 2.7, and 4.5 kg. The contact behavior at sliding rates of 0.05 and 0.005 cm/min were investigated. Approximately 80 individual sliding contact tests were performed; the contact surfaces were examined by optical microscopy (40X) and scanning electron microscopy after testing. Initially, specimens were fractured in four-point bending after contact testing to determine if the contact loads caused a reduction in strength. At the low normal forces used in this study, there was no measurable effect on strength.

In addition, several specimens with a glass layer applied were tested to compare the contact behavior of a known glassy surface with the behavior observed on the as-machined surfaces.

## 3.0 ELEVATED-TEMPERATURE CONTACT TEST APPARATUS AND PROCEDURE

The contact test apparatus previously used for high-temperature tests was difficult to align, had questionable reproducibility at low contact loads, and was limited to operation at 1100°C and below. A new contact apparatus was designed and constructed to correct these limitations.

Figure 5 shows the design of the new contact apparatus. Compared with the prior apparatus, load paths and fixtures have been simplified. This makes calibration easier and results in increased sensitivities, especially at the low contact loads required under the current program. The new furnace is lined with high-temperature fiber insulation and can be heated much more rapidly than the prior furnace, with a capability in excess of 1400°C. The clam-shell construction and swivel mounting allow the furnace to be moved out of the way for better alignment and calibration than was possible with the previous apparatus. Figure 6 is a photograph of the new test apparatus with the furnace opened to show placement of the test specimens.

To improve alignment and to eliminate excess movement of the test specimen in the test fixture and test apparatus, the specimens are machined to very close tolerances, as shown in Figure 7. Specimen B is held stationary during the test, and its 0.32-cm radius surface is held in contact with Specimen A. Specimen A is moved tangentially during the test, and its 0.64-cm flat surface is used as the test surface.

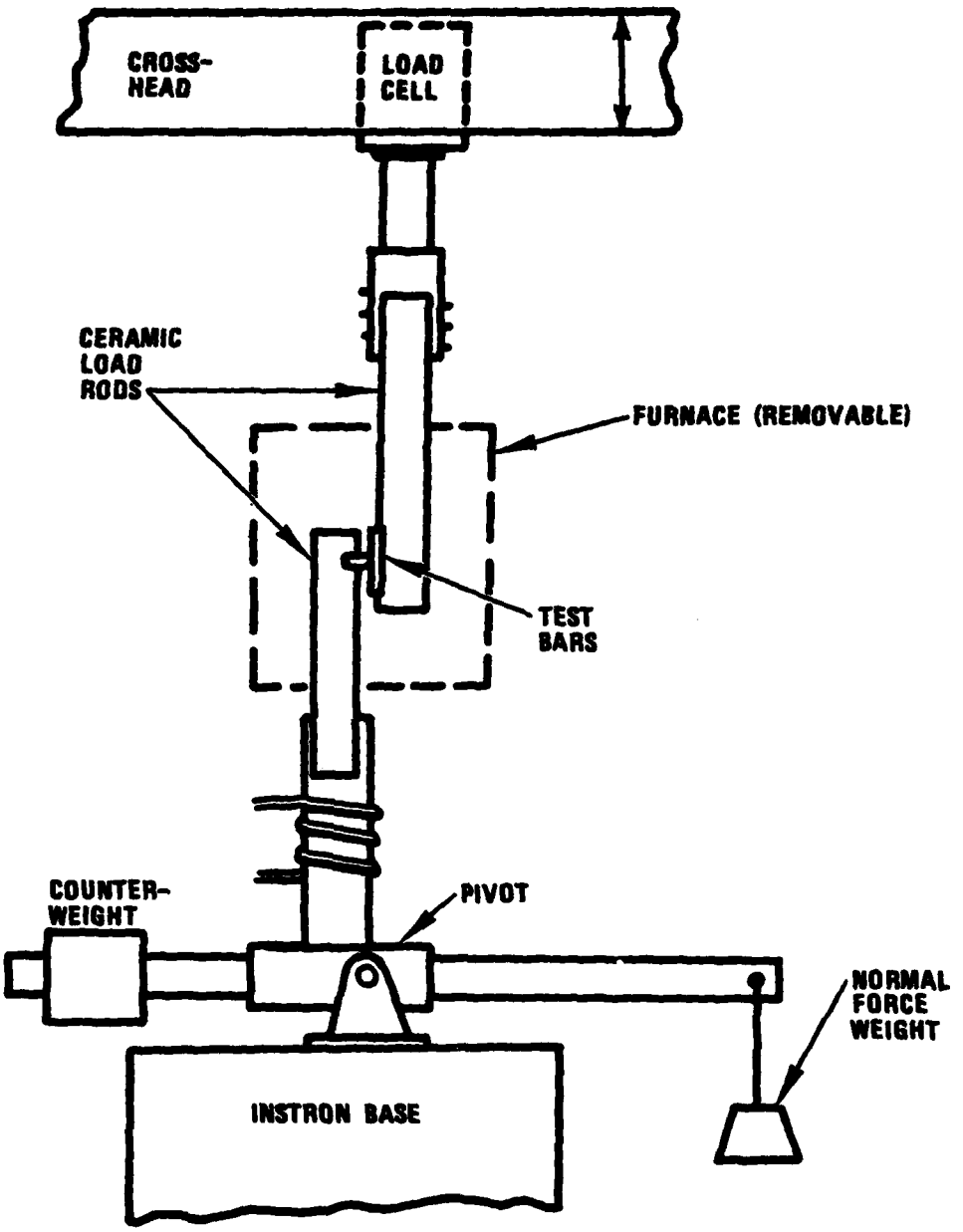


Figure 5. Design of New Contact Stress Rig.

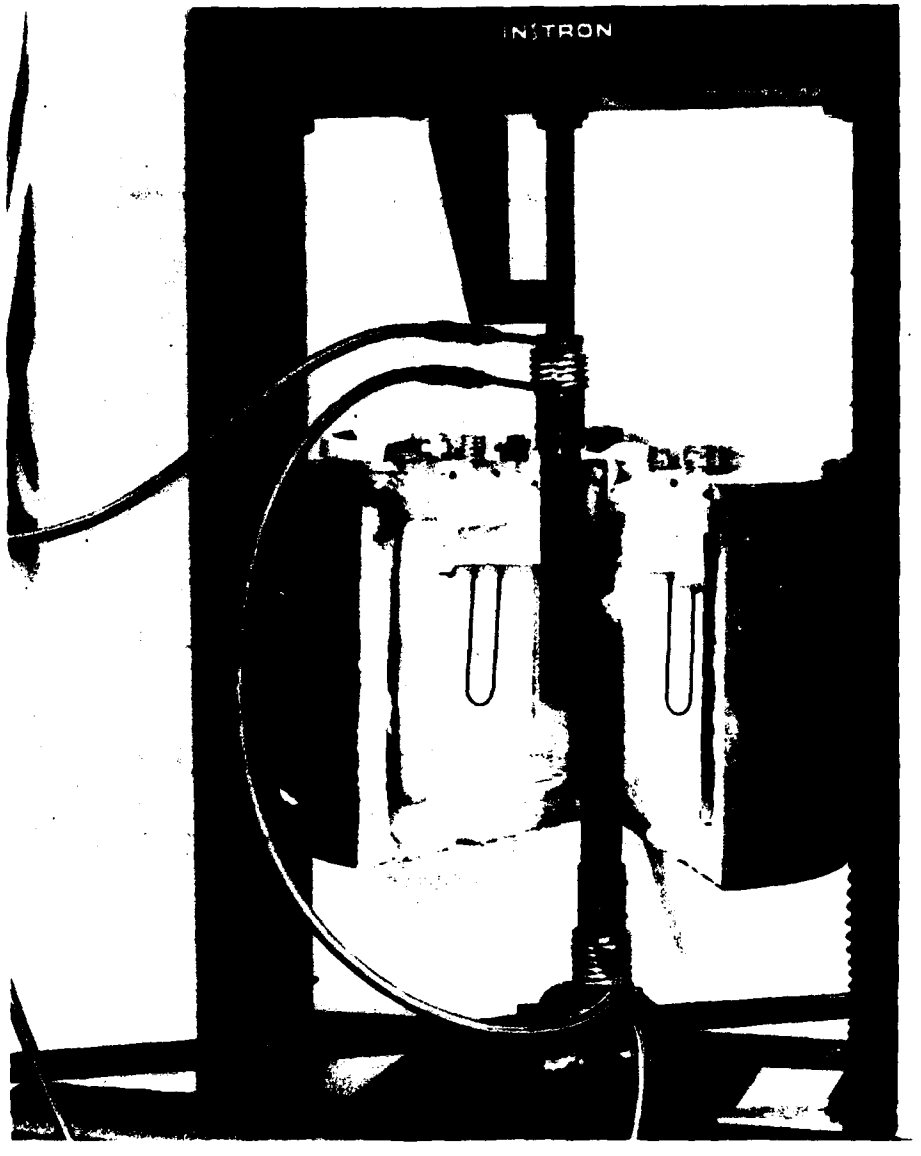


78424-7

Figure 6. New Contact Stress Rig.

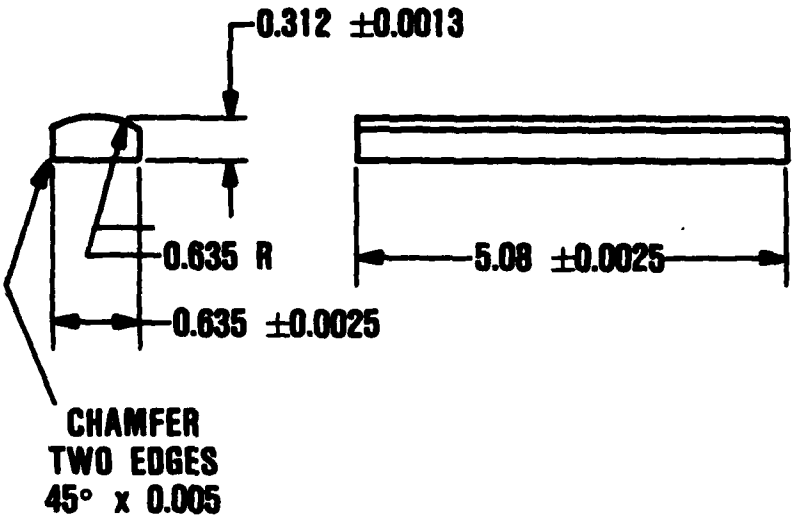


SPECIMEN A

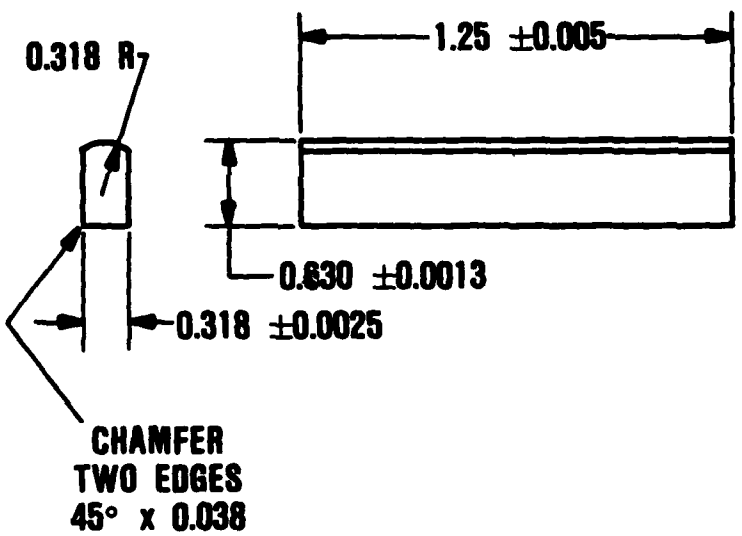


SPECIMEN B

DIMENSIONS, CM

Figure 7. Contact-Stress-Rig Test Bars.

Each experiment consisted of the following procedure. The specimens were placed in the test fixture not contacting each other. The furnace was closed around the test apparatus and heated to the desired temperature in approximately 15 to 20 minutes. When the furnace equilibrated at the test temperature, the normal force was applied. The specimens were held in contact by the normal force for a specified time; relative motion was then induced by the testing machine*, and the tangential force was measured by the load cell. The sliding distance (contact distance) is 0.076 to 0.15 cm for each test. The data obtained is in the form of a force/time curve, from which static, dynamic, and recovery forces could be determined. These measured forces were used to analyze the contact behavior.

After each test, the specimens were cooled to room temperature and examined visually (40X). Selected specimens were also examined by scanning electron microscopy.

*Instron Corp., Canton, MA.

## 4.0 TEST RESULTS

### 4.1 Friction Versus Temperature

The initial series of experiments consisted of measuring the friction at room temperature, 400°, 600°, 900°, and 1100°C for normal forces of 0.5, 1.4, 2.7, and 4.5 kg. All tests were performed at a sliding rate of 0.05 cm/min (the rate used for all previous contact studies), with a 30-minute hold time in contact.

Figure 8 shows typical force/time curves for four different temperatures. There is no clear delineation between static and dynamic behavior at temperatures of 600°C and below. At 900° and 1100°C, there is a distinct breakaway that defines the static coefficient of friction. The recovery force (Figure 9) increases with increasing temperature or normal force. The recovery force is a measure of the relaxation of the tangential force that takes place after the crosshead of the testing machine is stopped at the end of a dynamic test. The specimens move relative to each other, relieving the tangential force.

The results for this series of experiments are presented in Table 3; the results are plotted in Figure 10 in terms of static force. The static force increases slightly with temperature to 900°C for each of the normal forces. Above 900°C, there is a drastic increase in static force for normal forces of 1.4 and 2.7 kg, while specimens under 4.5-kg normal force do not exhibit this drastic increase. The 0.5-kg normal force situation shows a continuous increase in static force with temperature, initiating at ~600°C. If the contact behavior were purely elastic, there would be no increase in frictional force with increased temperature over the temperature range of interest. Therefore, these results suggest that some mechanism(s) other than elastic is contributing to the measured frictional force.

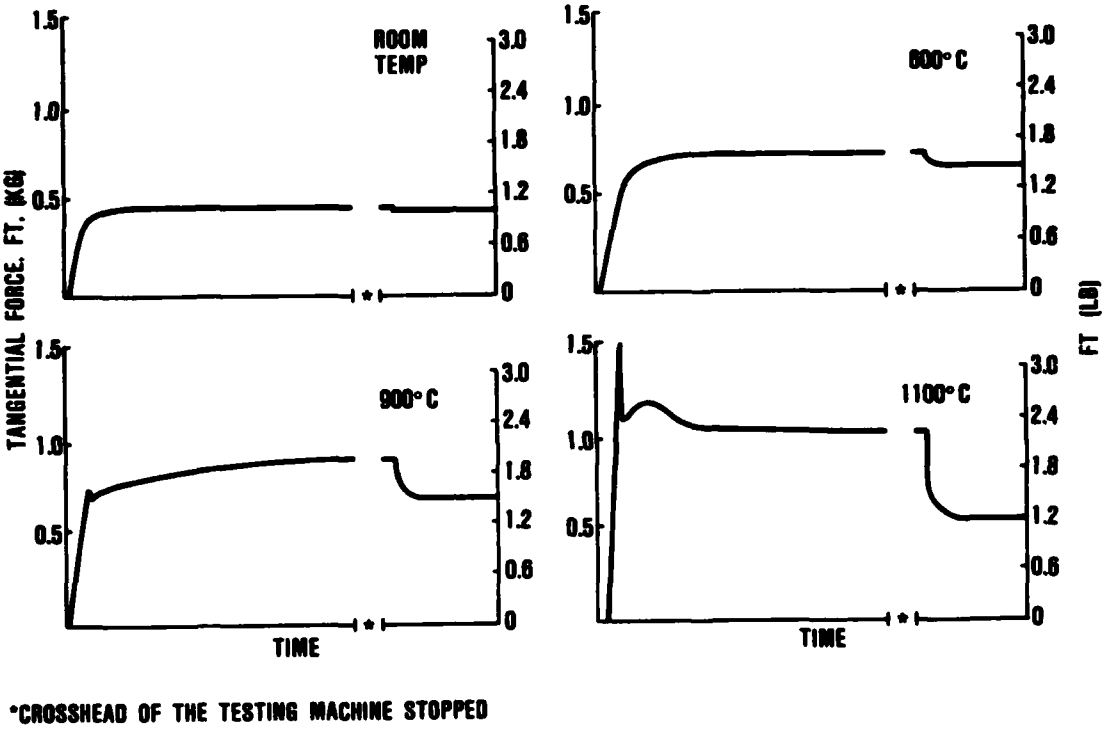


Figure 8. Force/Time Curves for 1.4-kg Normal Force.

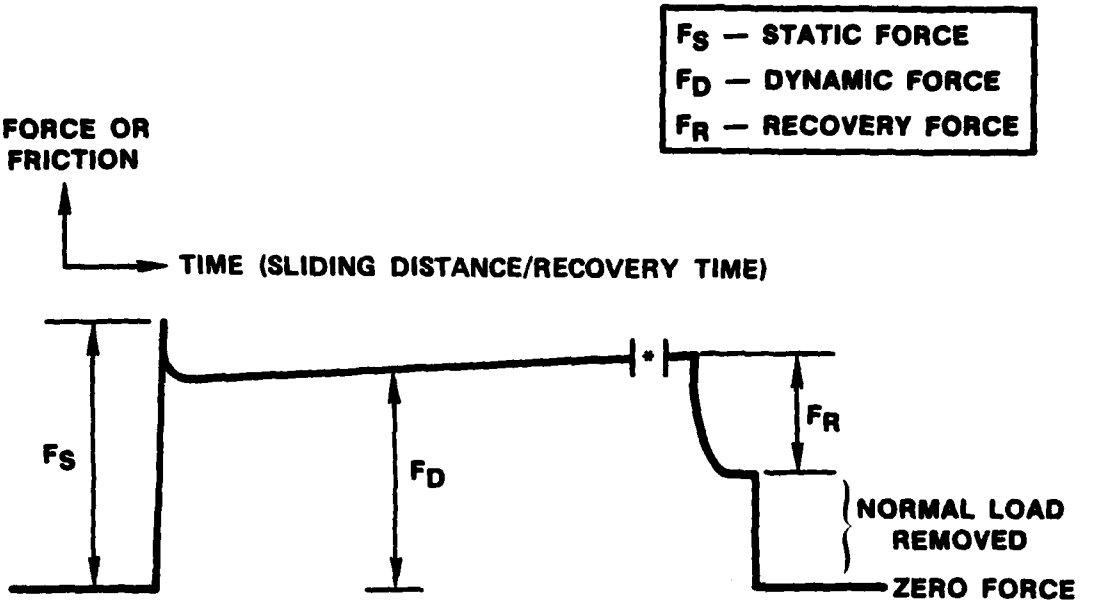


(A) HIGH-TEMPERATURE

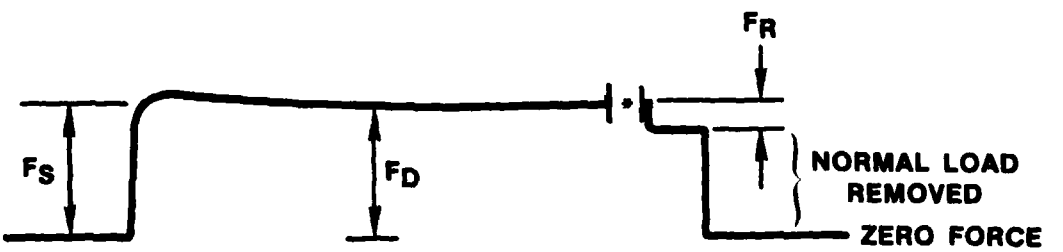


(B) LOW-TEMPERATURE

*CROSSHEAD OF THE TESTING MACHINE STOPPED

Figure 9. Schematic of Force/Time Curve for Contact Tests.

TABLE 3. RESULTS FOR LINE-CONTACT TESTING OF SASC ON SASC, SLIDING RATE = 0.05 CM/MIN.*

| Temperature (°C) | $F_N$ (kg) | $F_S$ (kg) | $\mu_S$ | $F_D$ (kg) | $\mu_D$ | $F_R$ (kg) | Strength** (MPa) |
|---|---|---|---|---|---|---|---|
| Room Temp | 0.5 | 0.14 | 0.30 | 0.14 | 0.30 | 0 | 321 |
| 400 | 0.5 | 0.14 | 0.30 | 0.25 | 0.55 | 0.02 | 309 |
| 600 | 0.5 | 0.18 | 0.40 | 0.36 | 0.80 | 0.05 | 321 |
| 900 | 0.5 | 0.36 | 0.80 | 0.36 | 0.80 | 0.09 | 309 |
| 1100 | 0.5 | 0.54 | 1.20 | 0.36 | 0.80 | 0.18 | 368 |
| Room Temp | 1.4 | 0.41 | 0.30 | 0.50 | 0.36 | 0 | 321 |
| Room Temp | 1.4 | 0.50 | 0.33 | 0.39 | 0.28 | 0 | - |
| 400 | 1.4 | 0.50 | 0.33 | 0.50 | 0.33 | 0.05 | 321 |
| 600 | 1.4 | 0.64 | 0.47 | 0.77 | 0.57 | 0.09 | 321 |
| 900 | 1.4 | 0.73 | 0.53 | 0.86 | 0.63 | 0.18 | 345 |
| 1100 | 1.4 | 1.63 | 1.20 | 1.04 | 0.77 | 0.50 | - |
| Room Temp | 2.7 | 0.73 | 0.27 | 0.91 | 0.33 | 0 | 333 |
| 400 | 2.7 | 0.91 | 0.33 | 1.00 | 0.37 | 0.09 | 321 |
| 600 | 2.7 | 1.27 | 0.47 | 1.36 | 0.50 | 0.14 | 274 |
| 900 | 2.7 | 1.36 | 0.50 | 1.50 | 0.55 | 0.27 | 309 |
| 1100 | 2.7 | 2.90 | 1.10 | 1.72 | 0.63 | 0.77 | 333 |
| 1100 | 2.7 | 3.08 | 1.13 | 2.13 | 0.78 | 1.00 | - |
| Room Temp | 4.5 | 1.22 | 0.27 | 1.45 | 0.32 | 0.09 | 368 |
| 400 | 4.5 | 1.81 | 0.40 | 2.27 | 0.50 | 0.23 | 321 |
| 600 | 4.5 | 1.68 | 0.37 | 2.27 | 0.50 | 0.32 | 334 |
| 900 | 4.5 | 2.45 | 0.54 | 2.81 | 0.62 | 0.82 | 240 |
| 1100 | 4.5 | 2.27 | 0.50 | 2.72 | 0.60 | 1.59 | 321 |

*Legend for column titles:

$F_N$ - Normal Force
$F_S$ - Static Force
$\mu_S$ - Static Friction
$F_D$ - Dynamic Force
$\mu_D$ - Dynamic Friction
$F_R$ - Recovery Force

**Room-temperature, four-point bond strength after contact test.

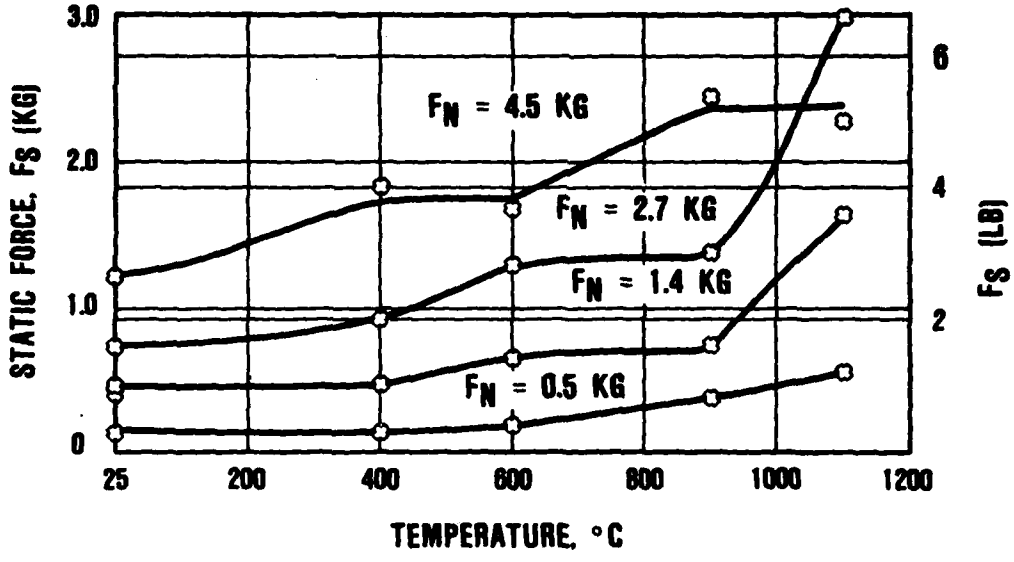


Figure 10. Static Force as a Function of Temperature (Line Contact, 0.05-Cm/Min Sliding Rate).

In terms of coefficient of static friction, there is a four-fold increase from room temperature to 1100°C for normal forces below 4.5 kg (Table 3). The elastic model for contact stress shows a strong dependence of the tensile stress at the contact interface on the coefficient of friction. Using the measured coefficients of static friction at 1100°C and the elastic model computer program developed in Reference 1, the predicted tensile stress for normal forces of 0.5 to 4.5 kg ranged from 408 to 990 MPa. These values exceed the baseline material strength (278 to 368 MPa), and should result in considerable surface damage and strength reduction if a purely elastic model pertains. However, the measured strengths of the specimens after contact testing (Table 3) show no measurable strength reduction. This provides further evidence that the high-temperature contact conditions are not purely elastic and that the previously developed elastic model required modification to include nonelastic effects.

The mechanism(s) contributing to the high measured coefficient of static friction is probably nonelastic in nature, along with the possibility of actual bonding of the test specimens during the 30-minute hold period. The contact surfaces of the specimens tested at 1100°C were examined by optical (40X) and scanning electron microscopy techniques and exhibited no evidence of bonding. However, there was evidence of a thin surface layer taking part in the contact behavior. Figure 11 is a scanning electron photomicrograph of a typical contact area after an 1100°C test.

Figure 12 presents the results of dynamic testing. As with the static situation, there is an increase in frictional force with increasing temperature. The coefficient of dynamic friction increases approximately two-fold from room temperature to 1100°C. This again suggests that mechanisms other than elastic are contributing to the contact behavior.

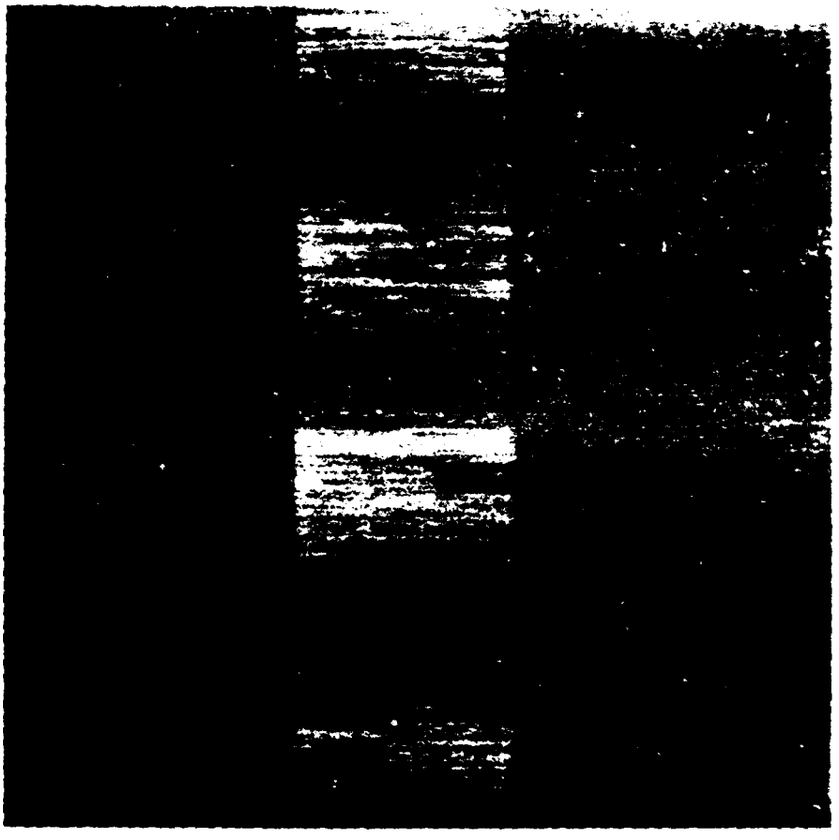

P800544

Figure 11. Scanning Electron Photomicrograph of Contact Area after Testing at 1100°C, 2.7-kg Normal Force.

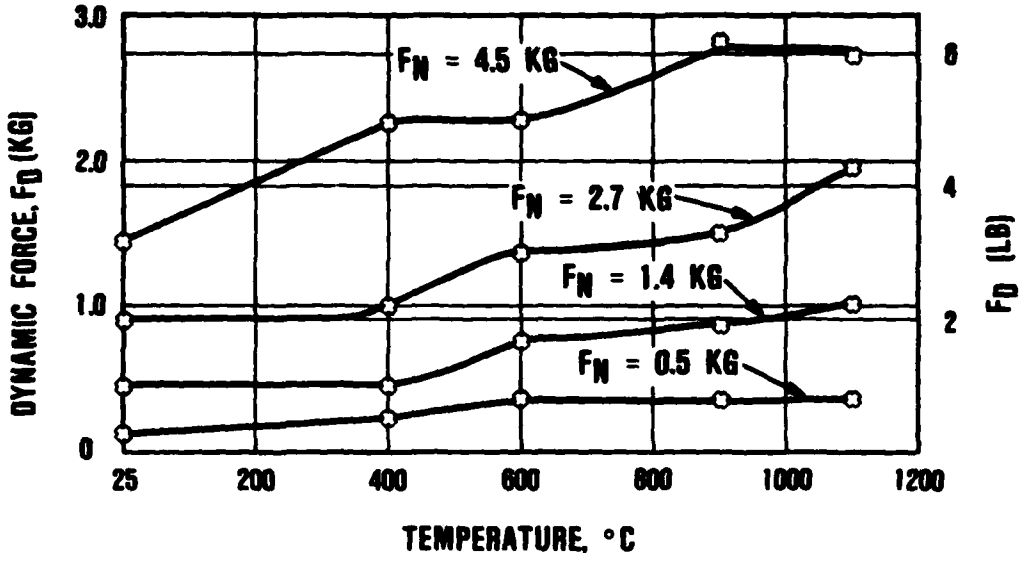


Figure 12. Dynamic Force as a Function of Temperature (Line Contact, 0.05-Cm/Min Sliding Rate).

At this point, two conclusions can be drawn. First, some mechanism other than elasticity is contributing to the measured friction, particularly at elevated temperatures. Second, the large increase in measured static force for 1.4- and 2.7-kg normal forces can probably be attributed to the amount of bonding that takes place during the 30-minute hold time. This bonding has not been quantified at this time primarily because of the difficulty in accurately determining the contact area.

This sequence of experiments provided additional data in the form of a recovery force. As can be seen in Table 3 and Figure 13, the recovery force is a strong function of both temperature and normal force. The magnitude of this force is more than can be explained elastically and is time-dependent (Figure 8), suggesting a nonelastic (viscous or viscoelastic) behavior. This behavior is similar to that observed during elevated deformation testing (creep) of ceramics.[7-11] In the case of creep, this behavior is attributed to a viscoelastic mechanism.[7-9]

## 4.2 Friction Versus Sliding Rate

If a viscous (time-dependent) mechanism is active, as suggested by the results reported earlier, then the measured effects (static and dynamic frictions and forces) should be dependent on the sliding (strain) rate. A series of contact experiments was conducted at a temperature of 1100°C; a sliding rate of 0.005 cm/min (as compared to 0.05 cm/min reported earlier); and normal forces of 0.5, 1.4, 2.7, and 4.5 kg. The results are presented in Table 4.

Figure 14 shows a typical force/time curve for a 0.005-cm/min sliding rate at 1100°C. The breakaway is distinct but not as abrupt as in the case of the 0.05-cm/min sliding test. Also, the dynamic trace is more uniform than in the 0.05-cm/min tests. As

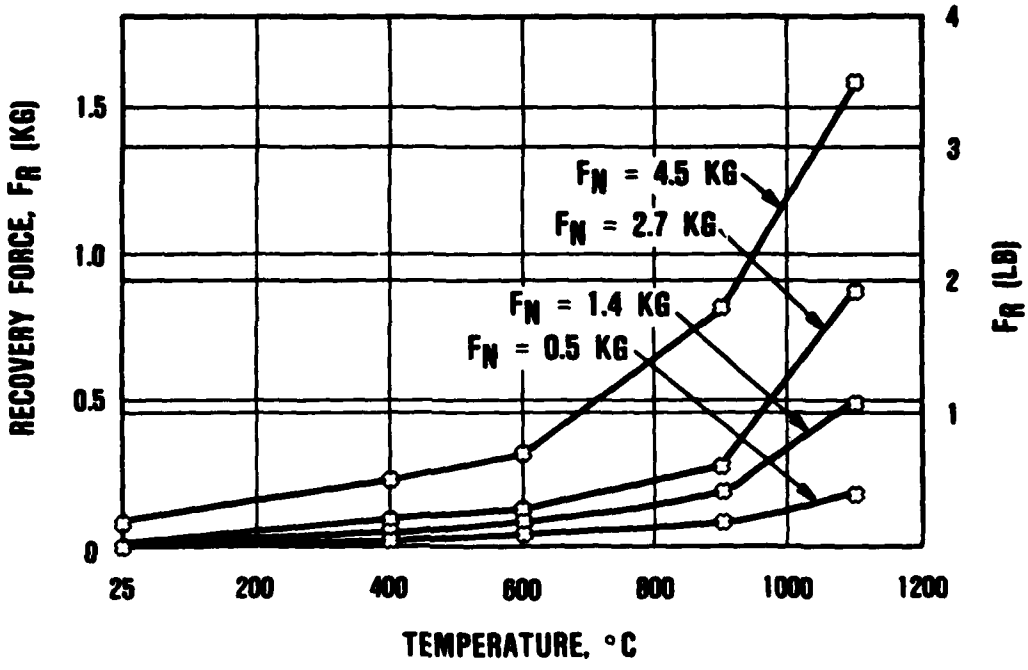


Figure 13. Recovery Force as a Function of Temperature (Line Contact, 0.05-Cm/Min Sliding Rate).

TABLE 4. RESULTS FOR LINE-CONTACT TESTING OF SASC ON SASC AT 1100°C, SLIDING RATE = 0.005 CM/MIN.*

| $F_N$ (kg) | $F_S$ (kg) | $\mu_S$ | $F_D$ (kg) | $\mu_D$ | $F_R$ (kg) |
|---|---|---|---|---|---|
| 0.5 | 0.64 | 1.40 | 0.36 | 0.80 | 0.18 |
| 0.5 | 0.54 | 1.20 | 0.41 | 0.90 | 0.14 |
| 0.5 | 0.59 | 1.30 | 0.41 | 0.90 | 0.23 |
| 0.5 | 0.54 | 1.20 | 0.50 | 1.10 | 0.23 |
| 0.5 | 0.64 | 1.40 | 0.50 | 1.10 | 0.23 |
| 1.4 | 2.00 | 1.50 | 1.36 | 1.00 | - |
| 1.4 | 1.54 | 1.13 | 1.00 | 0.73 | 0.50 |
| 1.4 | 1.32 | 0.97 | 1.09 | 0.80 | 0.50 |
| 1.4 | 1.36 | 1.00 | 1.09 | 0.80 | 0.54 |
| 2.7 | 3.36 | 1.20 | 2.63 | 0.96 | 1.00 |
| 2.7 | 2.72 | 1.00 | 2.31 | 0.85 | 0.86 |
| 2.7 | 2.90 | 1.06 | 2.54 | 0.93 | 1.00 |
| 2.7 | 3.08 | 1.13 | 2.40 | 0.88 | 0.91 |
| 4.5 | 4.58 | 1.01 | 3.40 | 0.76 | 1.27 |
| 4.5 | 4.72 | 1.04 | 4.08 | 0.90 | 1.36 |
| 4.5 | 4.54 | 1.00 | 4.08 | 0.90 | 1.27 |
| 4.5 | 4.99 | 1.10 | 3.85 | 0.85 | 1.36 |

*Legend for column titles:

$F_N$ - Normal Force

$F_S$ - Static Force

$\mu_S$ - Static Friction

$F_D$ - Dynamic Force

$\mu_D$ - Dynamic Friction

$F_R$ - Recovery Force

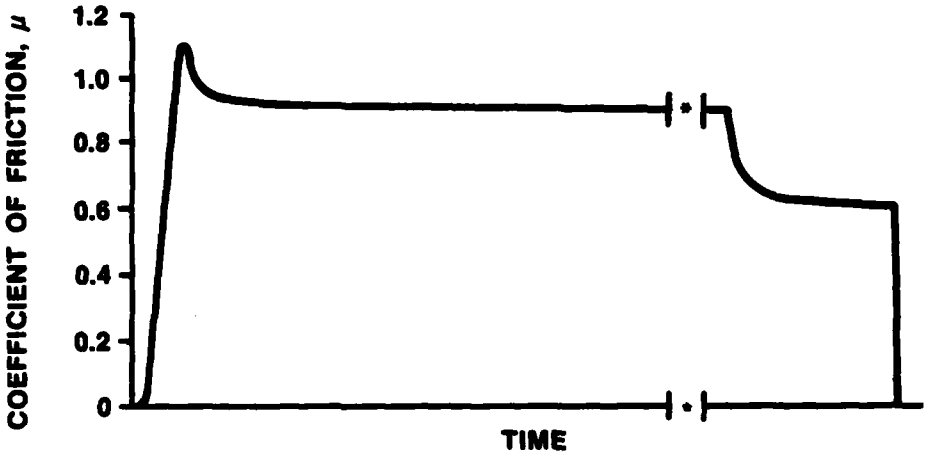


Figure 14. Force/Time Curve at 1100°C, 2.7-kg Normal Force, 0.005-Cm/Min Sliding Rate.

stated in Paragraph 4.1, there is no degradation of strength due to the low contact loads; therefore, flexure-strength measurements were not required. Tests discussed in this paragraph were multiple tests conducted on two test bars, with a different area of the test bar used for each test.

The measured coefficients of static and dynamic friction are essentially constant over the range of normal forces, although there is some indication that static and dynamic friction increased slightly for the 0.5-kg normal force. At normal forces of 2.7 kg or less, there was no measurable effect of strain rate; however, at 4.5-kg normal force, the effect of strain rate is a factor of 2. If there is a strain rate effect, it may require rates greater than an order of magnitude difference to produce a measurable effect at low normal forces. The data for this series of experiments does suggest a strain rate effect for high (greater than 4.5 kg) normal forces.

### 4.3 *Effect of Contact Time on Friction*

If bonding is taking place during the hold time prior to contact testing, static friction is expected to increase with hold time. A series of experiments was conducted at various hold times at 1100°C and 2.7-kg normal force. The results are presented in Table 5. The measured coefficient of static friction is essentially the same at 0- and 0.5-hour holding times, suggesting that the bonding effect is negligible at 0.5-hour holds (the conditions used in experiments discussed in Paragraph 4.2). After a 4-hour hold time, there is a small increase in the coefficient of static friction, but the coefficient of dynamic friction is essentially unchanged. This indicates that the degree of bonding may increase with longer contact times and that longer-term testing should be considered.

TABLE 5. EFFECT OF CONTACT TIME ON FRICTION FOR SASC ON SASC AT 1100°C, 2.7-KG NORMAL FORCE.*

| Hold Time (hr) | $F_S$ (kg) | $\mu_S$ | $F_D$ (kg) | $\mu_D$ |
|---|---|---|---|---|
| 0 | 2.95 | 1.08 | 2.27 | 0.83 |
| 0 | 3.18 | 1.16 | 2.27 | 0.83 |
| 0.5 | 2.90 | 1.06 | 1.72 | 0.63 |
| 0.5 | 3.08 | 1.13 | 2.13 | 0.78 |
| 4 | 3.63 | 1.33 | 2.04 | 0.75 |

*Legend for column titles:

$F_S$ - Static Force $F_D$ - Dynamic Force

$\mu_S$ - Static Friction $\mu_D$ - Dynamic Friction

## 4.4 Point Contact Versus Line Contact at Elevated Temperatures

If the measured coefficients of static and dynamic friction are controlled only by elastic behavior, the coefficients should not be a function of the area of contact; but if a viscous layer contributes to the measured coefficient, an increase in contact area should produce an increase in the static and dynamic friction due to the increased drag of the viscous layer. To evaluate the effect of contact area, several experiments were conducted at 1100°C in point contact for comparison with the results of line contact reported in Tables 3 and 4. The results of the point-contact tests are summarized in Table 6. In general, both coefficients of static and dynamic friction are higher in line contact than in point contact. This result would again suggest that a viscous mechanism is active during sliding contact of SASC at elevated temperatures.

TABLE 6. RESULTS FOR POINT CONTACT TESTING OF SASC ON SASC AT 1100°C.*

| $F_N$ (kg) | $F_S$ (kg) | $\mu_S$ | $F_D$ (kg) | $\mu_D$ | $F_R$ (kg) |
|---|---|---|---|---|---|
| Sliding Rate = 0.05 Cm/Min | | | | | |
| 1.4 | 1.08 | 0.80 | 0.77 | 0.56 | 0.27 |
| 2.7 | 1.63 | 0.60 | 1.13 | 0.41 | 0.45 |
| 4.5 | 3.17 | 0.70 | 2.04 | 0.45 | 0.81 |
| Sliding Rate = 0.005 Cm/Min | | | | | |
| 0.5 | 0.50 | 1.10 | 0.36 | 0.80 | 0.18 |
| 0.5 | 0.50 | 1.00 | 0.36 | 0.80 | 0.18 |
| 1.4 | 0.91 | 0.67 | 0.68 | 0.50 | 0.32 |
| 1.4 | 0.91 | 0.67 | 0.68 | 0.50 | 0.32 |
| 2.7 | 1.09 | 0.40 | 1.18 | 0.43 | 0.54 |
| 2.7 | 1.36 | 0.50 | 1.18 | 0.43 | 0.50 |
| 2.7 | 1.54 | 0.56 | 1.08 | 0.40 | 0.54 |
| 4.5 | 2.27 | 0.50 | 2.18 | 0.48 | 0.91 |
| 4.5 | 2.40 | 0.53 | 2.18 | 0.48 | 0.91 |

*Legend for column titles:

$F_N$ - Normal Force
$F_S$ - Static Force
$\mu_S$ - Static Friction
$F_D$ - Dynamic Force
$\mu_D$ - Dynamic Friction
$F_R$ - Recovery Force

## 4.5 Effect of Glazed Surface on Friction

If it is assumed that a viscous layer can contribute to the frictional behavior of SASC at elevated temperatures, it would be logical to expect the behavior to be magnified as the thickness of the layer increases. To evaluate the effect of a thick viscous layer, a glass layer (glaze) 0.0015-cm thick was applied to the surface of a SASC specimen and contact tested at 1100°C. Normal forces of 1.4 and 2.7 kg and a sliding rate of 0.05 cm/min were used for these experiments. Figure 15 shows a typical force/time curve for these tests. In both cases, the specimens exhibited a distinct, very abrupt breakaway with coefficients of static friction equal to 2.9 and 1.6 for normal loads of 1.4 and 2.7 kg, respectively. This shows that a viscous layer can contribute to an increase in the apparent static friction and that the effect is more pronounced as the normal force decreases. The coefficient of dynamic friction varied over a wide range during the test. This could be related to the change in contact area during the test, as shown in Figure 16.

The most significant information gained from these experiments is the effect of the glazed surface on the recovery force. The recovery force, which is a measure of the amount of tangential force relieved, was equal to essentially 100 percent of the tangential force. Therefore, tangential force was completely relieved, a result that would be expected if the behavior is viscous in nature. With the excess glassy layer on the specimen, it would be logical to assume that all of the behavior during testing was controlled by a viscous mechanism. If this is true, the recovery force measured during the tests reported in Paragraph 4.2 should be related to the magnitude of the viscous contribution to the contact behavior at elevated temperatures.

These experiments can also assist in explaining the apparent differences between results reported in Paragraph 4.2 and earlier

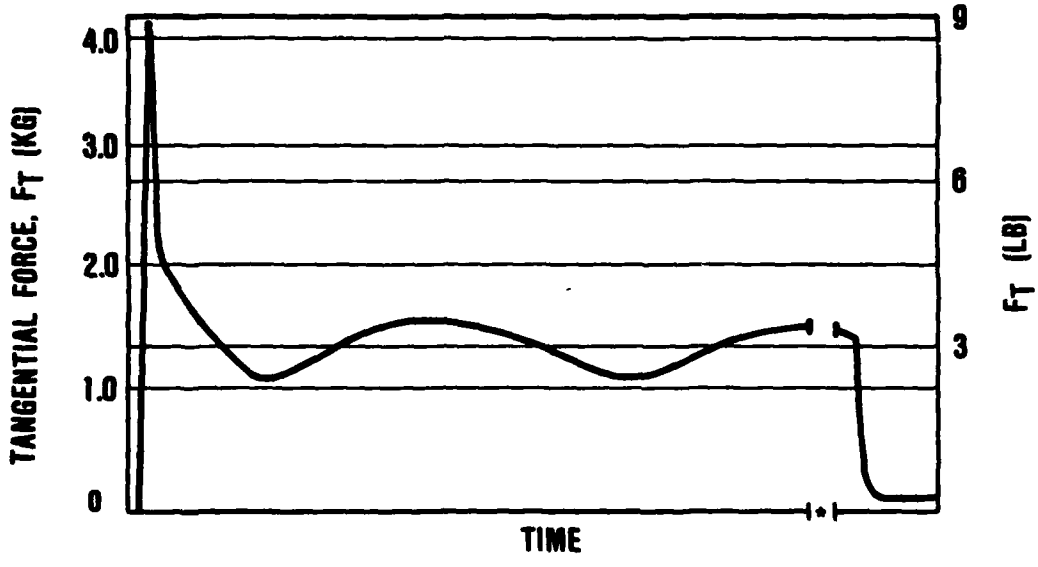


*CROSSHEAD OF THE TESTING MACHINE STOPPED

Figure 15. Force/Time Curve at 1100°C, 1.4-kg Normal Force for Glazed SASC.

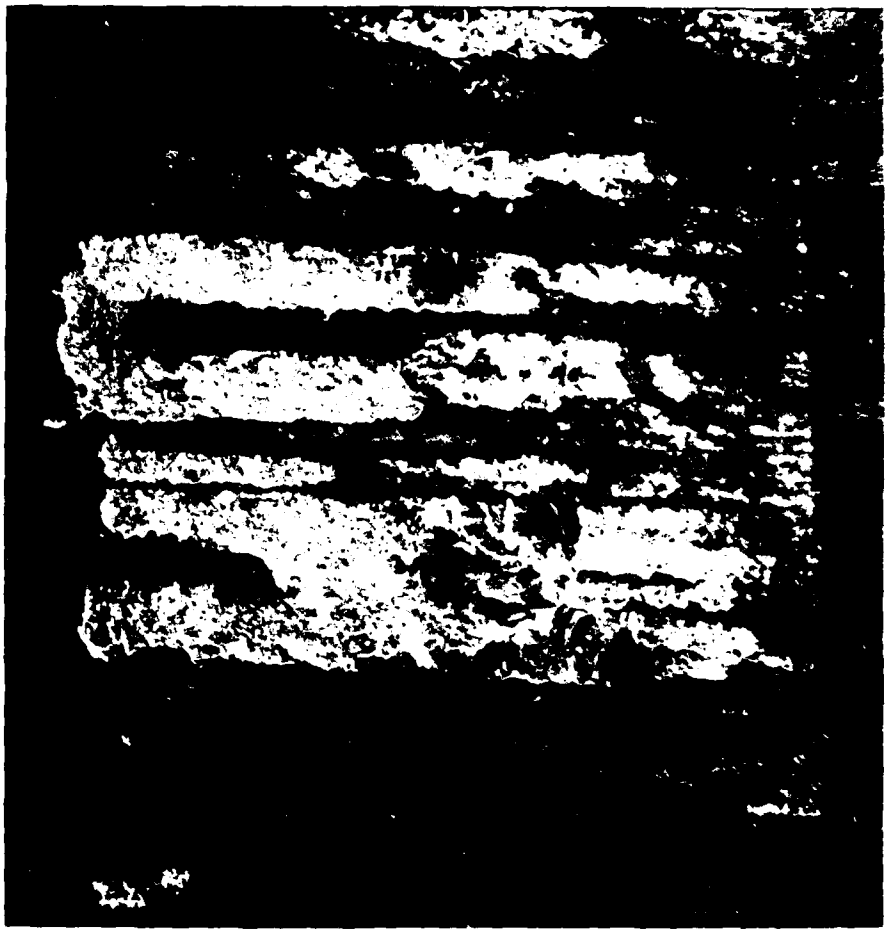

P80654-2

Figure 16. Scanning Electron Micrograph of Glazed Contact Surface after Testing at 1100°C, 0.05-Cm/Min Sliding Rate, and 2.7-kg Normal Force.

results presented in Section 1.0. In the earlier work, it was reported that the static friction at 1100°C increases as normal force decreases for normal forces less than 4.5 kg. Although the present work shows an increase in static friction at 1100°C for normal forces less than 4.5 kg, it does not show a continued increase for normal forces less than 2.7 kg. The difference in these results is probably related to the amount of glassy layer formed on the contact surfaces. In the earlier work, a definite glassy layer was observed (Figure 2), whereas in the present work, no distinct glassy layer was found.

Thus, based on earlier work and the results presented in this paragraph, it appears that the amount of glass present determines the relation between static friction and normal force at 1100°C. This suggests that if a glassy layer is present, the viscous component of static friction (and probably dynamic friction) becomes more dominant as the normal force is reduced.

## 5.0 CONCLUSIONS

Work accomplished during this reporting period leads to the following conclusions:

- The results reported strongly indicate that a viscous and/or viscoelastic mechanism is contributing to the contact behavior of SASC at elevated temperatures.

- The magnitude of the viscous effect is a function of contact area and thickness of the viscous layer.

- The recovery force appears to be related to the magnitude of viscous and/or viscoelastic contribution to contact behavior.

- More experimental data is needed to evaluate contact behavior (static and dynamic force, static and dynamic friction, and recovery force) as a function of contact area, thickness of the viscous layer, viscosity of the layer, and temperature. When this information is available, an analytical and computational model can be developed to account for the viscous behavior at the contact interface at elevated temperatures.

## 6.0 LIST OF REFERENCES


1. "Contact Stress Analysis of Ceramic-to-Metal Interfaces", Final Report Contract N00014-78-C-0547, September 21, 1979. Garrett Report No. 21-3239.

2. "Contact Stress Analysis of Ceramic-to-Metal Interfaces", Final Report Contract N00014-79-C-0867, September 2, 1980. Garrett Report No. 21-3690.

3. "Contact Stress Analysis of Ceramic-to-Metal Interfaces", Annual Report Contract N00014-80-C-0870, October 9, 1981. Garrett Report No. 21-4140.

4. D. W. Richerson, L. J. Lindberg, and C. Dins, AiResearch Report No. 76-212188(17), "Ceramic Gas Turbine Engine Demonstration Program", Interim Report No. 17 (Quarterly), May 1980, Navy Contract No. N00024-76-C-5352.

5. D. W. Richerson, W. D. Carruthers, and L. J. Lindberg, "Contact Stress and Coefficient of Friction Effects on Ceramic Interfaces" in Surfaces and Interfaces in Ceramic and Ceramic-Metal Systems, J. Pask and A. Evans, eds., Plenum Press, 1981, pp. 661-676.

6. D. W. Richerson, L. J. Lindberg, W. D. Carruthers, and J. Dahn, "Contact Stress Effects on $Si_3N_4$ and SiC Interfaces", Ceramic Engineering and Science Proceedings, July-August 1981.

7. R. M. Arms and J. K. Tien "Creep and Strain Recovery in Hot-Pressed $Si_3N_4$, J. of Mat. Sci. 15 2046 (1980).

8. F. F. Lange, D. R. Clarke, and B. I. Davis, "Compressive Creep of $Si_3N_4$/MgO Alloys, Part 2 Source of Viscoelastic Effect", J. of Mat. Sci. 15 611 (1980).

9. F. F. Lange, D. R. Clarke, and B. I. Davis "Compressive Creep of $Si_3N_4$/MgO Alloys, Part 1 Effect of Composition", J. of Mat. Sci. 15 601 (1980).

10. F. H. Clews, J. M. Richardson, and A. T. Green, "The Behavior of Refractory Materials Under Stress at High Temperatures", Trans. Brit. Ceram. Soc. 45, 161 (1956).

11. R. Morrell and K. H. G. Ashbee, "High Temperature Creep of Lithium Zinc Silicate Glass-Ceramics, Part 2 Compression Creep and Recovery", J. of Mat. Sci 8 1271 (1973).

## 7.0 LIST OF REPORTS/PUBLICATIONS

The following reports/publications have been presented during the period of this contract:

- "Analytical and Experimental Evaluation of Biaxial Contact Stress," by D. W. Richerson, D. G. Finger, and J. M. Wimmer, published in Fracture Mechanics of Ceramics, Volume 5.

- "Contact Stress Analysis of Ceramic-to-Metal Interfaces", Annual Report for Contract N00014-80-C-0870, October 1981, Garrett Report No. 21-4140.

- "Contact Stresses at Ceramic Interfaces," by D. W. Richerson, published in Nitrogen Ceramics II.

- "Cyclic Rig and Engine Testing of Ceramic Turbine Components," by D. W. Richerson, K. M. Johansen, P. M. Ardans, and K. P. Johnson, published in Ceramic Engineering and Science Proceedings.

- End-of-the-Year Letter Report on ONR Contract N00014-80-C-0870, October 1982.